AKADÉMIAI KIADÓ

UNIVERSITY of DEBRECEN

International Review of Applied Sciences and Engineering

14 (2023) 3, 325–341

DOI:
10.1556/1848.2022.00556

ORIGINAL RESEARCH PAPER

A hybrid DMO-RERNN based UPFC controller for transient stability analysis in grid connected wind-diesel-PV hybrid system

K. Thanigaivel*, S. Ramesh and K. Karunanithi

Department of Electrical and Electronics Engineering, Vel Tech Rangarajan Dr. Sagunthala R&D Institute of Science and Technology (Deemed to be University), Avadi, Chennai, India

Received: July 6, 2022 • Accepted: November 17, 2022
Published online: March 20, 2023

ABSTRACT

In this paper, a novel hybrid technique is proposed for transient stability analysis on grid connected Wind-Diesel-PV hybrid system. The proposed hybrid methodology is combination of the dwarf mongoose optimization algorithm (DMO) and the recalling enhanced recurrent neural network (RERNN) named DMO-RERNN. The main purpose of this work is to consider various elements on hybrid system for the analysis of transient stability according to different conditions. The voltage profile of hybrid system is enhanced using the proposed unified power flow controller (UPFC), which also has higher performance improving transient performance compared to the conventional ANN, PI and fuzzy-sliding mode controller. Considering the proposed technique, DMO is used to find the optimal global solution for the fault predicted by the RERNN approach. The proposed system is executed on MATLAB work platform; its performance with existing systems is analyzed. The result proves that the proposed hybrid technique based UPFC controller provides better results compared with other existing technique. The efficiency of the PI is 82.136, ANN is 77, Fuzzy Sliding Mode is 65.097% and proposed technique is 97.99038%.

KEYWORDS

transient stability, grid connected hybrid system, voltage profile, global solution, load, fault, UPFC performance, controllers

1. INTRODUCTION

In central power system, an advanced Distributed Generation (DG) technology, like fuel cell (FC), wind turbine (WT), photovoltaic (PV) are used as an alternate energy. According to the requirement of the situation, DG achieves customers' demand in grid-connected and extra power generation given to grid to increase reliable power distribution. Unreliable and PQ problems arise in the power generation of wind and PV due to the undesired environmental characteristics variation of wind speed as well as solar radiations. To enhance the dependability of power distribution, the sources are needed to connect with typical power generating sources [1, 2]. Wind–diesel-photovoltaic systems are highly available hybrid system, where the wind turbine is linked to the diesel generator along photovoltaic system to deliver power in rural areas. Generally, by choosing synchronous generator (SG), performance improvement is achieved to operate diesel generator [3–7]. When compared with SG, the induction generator is much better because of its rugged characteristics and it is essential to consider the reactive power during the operation [8–10].

Induction generators and load-connected photovoltaics are considered as difficult, wherever the induction generators and loads require the reactive power delivered to SG and PV. The SG and PV inverters cannot satisfy the demand and generate a gap between demand as well as output of reactive power. It causes voltage stability problems. The capacitor banks are utilized to enhance voltage stability and manage reactive power [11–13]. The fixed

*Corresponding author.
E-mail: thanigaivelme@gmail.com

AKJournals

capacitor does not deliver the reactive power requirement. Henceforth, the reactive power compensation is achieved by alternatively using AC transmission system devices, like Static VAR Compensator (SVC), Unified Power Flow Controller (UPFC), Static Synchronous Compensator (STATCOM), [14–21]. These devices are utilized under the study of the angular and voltage stability of power system [22]. The reduced order linear system is achieved by the feedback linearization dynamic stability design technique by transforming the dynamics of the nonlinear system into a linear one. Here, a linear controller is considered in the design; due to this autonomous hybrid system becomes stable and has zero dynamics.

The controllers are modeled by utilizing the adaptive control methods [23]. In the robotic application as well as the semi-active suspension system, the sliding mode control (SMC) is utilized to make different structure [24]. The main feature of this SMC is to maintain the stability. The controller may be managing the modeling incorrectness. A fuzzy-PI control is recommended by many researchers that is another adaptive control method. A Hybrid DMO-RERNN based UPFC Controller is proposed to obtain superior performance subject to accuracy, overshoot and settling time. The foremost purpose of this work is to control reactive power using proposed DMO-RERNN based UPFC Controller for the better damping control on wind–diesel-photovoltaic hybrid system. The organization of this work is shown in Fig. 1.

Objectives and Contribution:

(a) A novel hybrid system is proposed for transient stability analysis on grid connected Wind-Diesel-PV hybrid system using hybrid system. The hybrid technique is a combination of dwarf mongoose optimization algorithm (DMO) and the recalling enhanced recurrent neural network (RERNN) named DMO-RERNN technique. At MATLAB/Simulink working platform, the proposed system proficiency is evaluated by relating with existing schemes.
(b) Considering the proposed technique, DMO is used to find optimal global solution for the fault predicted by the RERNN approach.
(c) The efficiency of the PI is 82.136, ANN is 77, Fuzzy Sliding Mode is 65.097% and the proposed technique is 97.99038%.

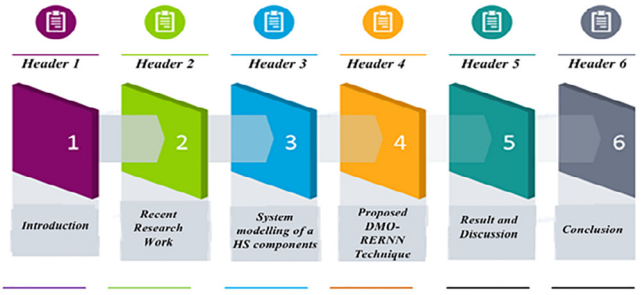

Fig. 1. Organization of work

2. RECENT RESEARCH WORK

In previous studies, the stability analysis in self-governing hybrid system using different techniques and aspects were explained. Some of them are revised here;

Wang et al. [25] presented an online power system transient stability assessment (TSA) issue using two-class classification problem. Here, a core vector machine (CVM) was used to tackle limitation via large phasor measurement unit (PMU) data. At first, offline training and online application framework were developed under selection, offline training, online application. PMU big data generation was involved by time domain simulation, training and testing of CVM model. Simultaneously, the online application procedure included the collection of PMU-specific big data in real time using the PMU data center interface and feature calculation program. The CVM-based assessment algorithm was much better than other support vector machines based on time consumption and space complexity.

Kassem and Abdelaziz [26] have suggested a firefly optimization approach to design the optimal control voltage stability of stand-alone hybrid renewable production unit depends on reactive power. The PMIG operated by wind turbine, also with the help of diesel engine, the synchronous generator was operated. In the system, the terminal bus voltage was stabilized via managing the reactive power by utilizing a STATCOM. By altering the total reactive power it was possible to stabilize the terminal voltage caused by the influence of the reactive power. The main objective was accomplished by restricting the STATCOM phase angle. System performance efficiency was obtained by comparing system control including model predictive, robust H, and classical PI control. Haruni et al. [27] have suggested a dynamic process along control approaches of hybrid Wind-Diesel-battery energy storage base power distribution amid the hybrid system components were achieved through the control strategies developed the system. The load and power demand generated from the wind turbine were managed by the battery energy storage system. During low wind condition a diesel generator was utilized in the wind energy conversion system to deliver sufficient power. A power generation strategy was implemented in case of low wind condition.

Shezan et al. [28] have explained the world's massive population, specifically in the emerging countries, was living in the rural areas. Actually, the rural areas were geographically isolated as regards grid connection. The complexities in providing these facilities were solved by renewable energy on off-grid hybrid energy system. Therefore, a system was modeled and simulated to help less community deeming an average load demand. Jamil et al. [29] have suggested increasing power quality for efficient power transmission on grid-connected solar PV-wind power systems. The hybrid system included a renewable energy according to PV power generation system and wind energy conversion system. The system was influenced by common disturbances on AC loads and power output. These disturbances were the reason for

power mismatch, voltage instability and power quality problems. These limitations were overcome by neglecting the gap with an adjustable reactive power source. Lee and Wang [30] have elucidated autonomous hybrid renewable energy power generation/energy storage system linked with isolated loads utilizing time-domain simulation. The frequency domain analysis of the hybrid system contains a diesel engine generator. The essential amount of hydrogen for FCs was generated using an aquatic electrolyzer by absorbing part of the energy produced by photovoltaic or wind turbines. According to different operating points and disturbance condition, a time domain technique was developed to obtain balance condition in system power frequency. Baghdadi et al. [31] have illustrated the investigation of efficiency of hybrid PV-Wind-Diesel-Battery configuration as a function of hourly measurements of the Adrar climate. In the beginning of the designing the system was optimized via HOMER software. Based on the renewable resources potential and energy demand the optimization process took place. Next, a mathematical model was developed according to different operation strategies to validate the efficient energy management.

Agarala et al. [32] have realized simple and innovative control system called automatic reactive power support (ARS) for single and combined renewable sources to improve system stability. Permanent Magnet Synchronous Generator (PMSG) and Doubly Fed Induction Generator (DFIG) were deemed from wind generators in this paper for comparison. Moreover, an improvement of transient stability was carried out, cultivating the critical clearance of three-phase fault on power system. Tian et al. [33] have clarified dual-stream CNN algorithm on deep learning, take the power of every node and line as input, quickly recognize the key oscillation modes of power system, and make qualitative assessment. D. Rakesh Chandra et al. [34] have postulated that the effect of DFIG on TS of grid-connected power system has been examined, to improve the TS of system. Here, the proposed TS analysis was executed on Reliability Test System (RTS)-24 bus system.

2.1. Background of research work

Recent studies show that hybrid system transient stability analysis was a major factor. System transient stability was affected using sudden load removal, line switching operations; system failure, etc. In such case, a data mining algorithm called core vector machine (CVM) based assessment algorithms was considered and has advantages, such as least time consumption and space complexity. To provide sufficient powers to the load power generation, a technique was utilized which was able to function during low wind condition. Different approaches were utilized to operate under dynamic and steady state condition. Even though the above-mentioned techniques have advantages, some limitations in achieving system power-frequency balance condition. The Static VAR Compensator (SVC) and UPFC were considered as the best device in reactive power compensation and voltage maintenance support. SVC was utilized to recover the power quality issues on the grid connected hybrid system according to reactive power control. However, the SVC and STATCOM exhibit better performance but it was difficult to maintain the system stability. These restrictions have inspired to do this investigation work.

3. SYSTEM MODELLING OF A HYBRID POWER SYSTEM COMPONENTS

Hybrid Power System (HPS) is a stand-alone electricity generation system utilized to supply power to the grid or on-site. By integrating various energy sources into one supply system, it leads hybridization technology to make use of local obtainable renewable energy sources to generate electric power. The proposed hybrid system is displayed in Fig. 2. Here, the induction generator and SG are used to deliver active with reactive power to the induction generator and the load using proposed DMO-RERNN-based UPFC controller [35]. Photovoltaic energy is considered in the proposed system to enhance the system performance. According to target power factor, the reactive power delivered or absorbed via photovoltaic system. In WECS, SG with IEEE type 1 excitation system is deemed and operates a local network for the induction generator. The mathematical modelling and various subsystems like wind diesel PV, FACTS controllers (SVC, STATCOM and UPQC) are defined as below:

$$Q_{PV} + Q_{SG} + Q_{CON} = Q_L + Q_{IG} \tag{1}$$

where the reactive power produced by PV denoted as Q_{PV}, reactive power produced SG is represented as Q_{SG}, the reactive power generated by controller denoted as Q_{CON}, the reactive power needed using load is mentioned as Q_L, the needed reactive power using induction generator is defined as Q_{IG}.

A change occurs in the load $_C$ causes all the parameters in the reactive power, which is represented as:

$$\Delta Q_{PV} + \Delta Q_{SG} + \Delta Q_{CON} = \Delta Q_L + \Delta Q_{IG} \tag{2}$$

The excessive reactive power influences the system voltage by maximizing the induction generator electromagnetic energy absorption and emerging the reactive load consumption of system. The excessive reactive power of system is expressed as:

$$\Delta Q_{PV} + \Delta Q_{SG} + \Delta Q_{CON} - \Delta Q_L - \Delta Q_{IG} \tag{3}$$

By rewriting the equation, the differential and Laplace forms are represented as:

$$\Delta Q_{PV} + \Delta Q_{SG} + \Delta Q_{CON} - \Delta Q_L + \Delta Q_{IG} = \frac{d}{dt}(\Delta E_m) + D_V \Delta V \tag{4}$$

$$\Delta V(S) = \frac{K_V}{1 + ST_V}[\Delta Q_{SG}(S) + \Delta Q_{CON}(S)] + \Delta Q_{PV}(S) - \Delta Q_L(S) - \Delta Q_{IG}(S)] \tag{5}$$

here

$$T_V = (2H_r/D_V)V^O \text{and } K_V = (1/D_V)$$

The dynamic behaviors of WTG, DEG, PV are analyzed utilizing high-order mathematical model with nonlinearity

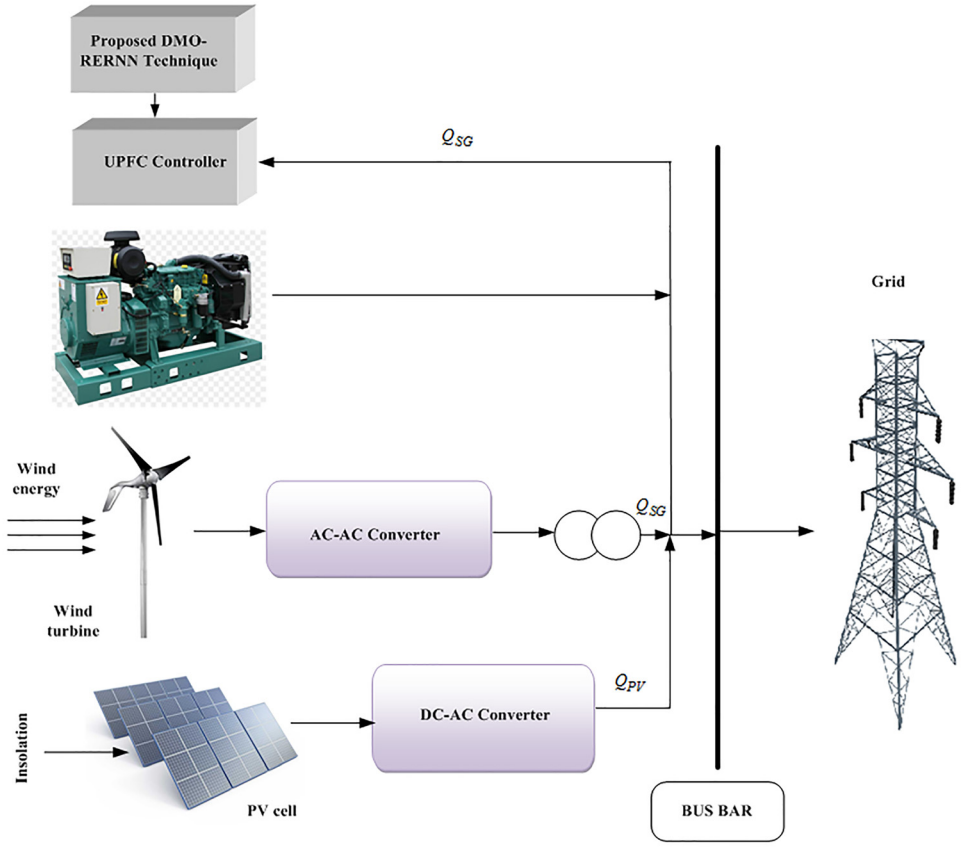

Fig. 2. Block diagram of proposed system

and it consist of power conditioners and controllers. In case of transient analysis, the mathematical model of system components is assumed [36].

3.1. Modelling of photovoltaic system

The photovoltaic cell is also called as p-n junction device that is utilized to convert the count of incidence solar radiation into electric power. A photovoltaic small signal equivalent mode is considered to deliver the reactive power to the proposed system [37].

$$F = V + JY_S I \tag{6}$$

$$F\sin(\delta) = Y_S I\cos(\phi) \tag{7}$$

where ϕ denotes the power angle amid grid and inverter output, δ represents load angle amid grid voltage (V) and inverter output voltage (F).

The active power given to the grid by the converter may be illustrated as:

$$P = VI\cos(\phi) = \frac{VF}{Y_S}\sin(\delta) \tag{8}$$

The reactive power given to the grid by the PV is expressed as:

$$Q = \frac{VF}{Y_s}\cos(\delta) - \frac{V^2}{Y_S} = \frac{V}{Y_S}(V\cos(\delta) - V) \tag{9}$$

3.2. Modelling of wind energy system

In the proposed hybrid system, WT is deemed as an important power source and the electric power generated through the wind turbine is based on wind speed [38]. Wind speed is separated into three groups: rated speed, cutoff speed, and cutout speed. WT power is largely based on the rate of change of kinetic energy:

$$P = \frac{dE}{dt} = \frac{1}{2}\frac{dm_a}{dt}v_W^2 \tag{10}$$

here $\frac{dm_a}{dt} = \rho a v_W$ describes the mass flow rate, a denotes wind area, ρ denotes air density. Equation (10) can be rewritten as:

$$P = \frac{1}{2}\rho a v_W^3 \tag{11}$$

According to the flow of upstream and downstream wind powers, the removed mechanical power is decided and can be set as:

$$P_W = \frac{1}{2}\rho a v_W\left(v_U^2 - v_D^2\right) \tag{12}$$

here v_U describes the velocity of wind in upstream, v_D signifies velocity of wind in downstream and above equation is rewritten as:

$$P_W = \frac{1}{2}\rho a r_p v^3 \tag{13}$$

where P_W refers to mechanic power on air flow, r_p denotes power coefficient depending tip speed ratio and blade pitch angle.

3.3. Modelling of diesel generator

When the load requirement is not compromised using other renewable energy system or the batteries then it is essential to consider diesel generator on HRES. The diesel generator is selected based on the sort and nature of load. The engine generator rated capacity needed to install is based on the following criteria such as,

- In case of directly connecting the diesel generator to the load, the rated capacity of generator should be similar.
- When using the diesel generator from battery charger, it important to note that the generated current of the generator must not be superior to $C_{Ah}/5$ A.

The diesel generator general efficiency is expressed as:

$$\eta_{overall} = \eta_{brake\ thermal} \times \eta_{generator} \tag{14}$$

here, $\eta_{\text{brake thermal}}$ defines the brake thermal of diesel engine. At hybrid power system the diesel generator is designed to achieve the required demand. Due to absence of peak demand the diesel generator is utilized to obtain load requirements and to charge battery.

3.4. Induction generator model

The reactive power generated from SG and the power demand of induction generator based on variation of the wind speed. The svc controller state space equation is expressed in a standard form which is given below:

$$y = [A]\overline{y} + [B]\overline{u} + [C]\overline{p} \tag{15}$$

$$\overline{y} = \left[\Delta F_{fd} \Delta V_a \Delta V_f \Delta E_q^{/} \Delta B_{SVC} \Delta B_{SVC}^{/} \Delta\alpha \Delta V\right]^T \tag{16}$$

$$\overline{u} = \left[\Delta V_{ref}\right] \tag{17}$$

$$\overline{p} = \left[\Delta Q_L\ \Delta PIW\right]^T \tag{18}$$

The calculation of matrix $[A], [B], [C]$ is similar order represents $\overline{x}., \overline{u}a$ and $\overline{p}$.

3.5. Mathematic model of SG

SG is considered to be the primary source of power and alternative to grid power, and SG is used to deliver reactive power. When connected to WT, the rotor speed is secured by properly controlling the SG. The SG equation is expressed as:

$$Q_{SG} = \frac{\left(F_q^{/} V\cos\delta - V^2\right)}{X/d}\,(\text{Transient}) \tag{19}$$

The above equation is rewritten as,

$$\Delta Q_{SG} = \frac{V\cos\delta}{Y/d\Delta F/q} + \frac{F/q\,\cos\delta - 2V}{Y/d\Delta/V} \tag{20}$$

Using Laplace equation may be rewritten as,

$$\Delta Q_{SG}(S) = K_a \Delta F/q(S) + K_b \Delta V(S) \tag{21}$$

here

$$K_a = \left(V\cos\delta \Big/ Y/d\right) \tag{22}$$

$$K_a = \left(F/q\cos\delta - 2V \Big/ Y/d\right) \tag{23}$$

3.6. Modelling of excitation system

The excitation system is utilized to generate direct current and it is used to drive the synchronous machine. The excitation system has the ability to manage the field voltage along field current, which is defined using individual time constant automatic high gain AVR System. Several sorts of excitation systems are available, in which, IEEE excitation system is considered in the hybrid system. The mathematical expression for the excitation system is defined by

$$\dot{F}_{fd} = \left(-F_{fd} + K_A(V_{ref} - V) \Big/ T_A\right. \tag{24}$$

3.7. Flux linkage of SG

The flux linkage equation for round rotor synchronous motor is expressed as:

$$\frac{d}{dt}\left(\Delta F_q^{/}\right) = \frac{\left(\Delta F_{fd} - \Delta F_q\right)}{T_{do}^{/}} \tag{25}$$

$$F_q = \left(\frac{Y_d}{Y_d^{/}}\right) F/q - \left(\frac{Y_d - Y_d^{/}}{Y/dV\cos\delta}\right) \tag{26}$$

The Laplace transform is applied in order to obtain a small incremental change which is expressed as:

$$(1 + ST_G)\Delta F/q(s) = K_e \Delta F_{fd}(s) + K_f \Delta V(s) \tag{27}$$

here

$$T_G = \left(Y_d^{/} T_{do} \Big/ Y_d\right), K_e = \left(Y_d^{/} \Big/ Y_d\right)$$
$$\text{and } K_f = \left(\left(Y_d - Y_d^{/}\right)\cos\delta \Big/ Y_d\right)$$

3.8. Unified power flow control

It is utilized to manage reactive power compensation, and it is utilized to manage reactive power coordinates using robust control models in the proposed hybrid system. Figure 3 implicates that block diagram of UPFC controller. The UPFC's series and shunt impedances are considered as pure reactance [39]. The shunt voltage sources are represented as P_{sh}, Q_{sh} and the series voltage sources are denoted as P_i, Q_i, P_j and Q_j. In UPFC, the injected power is depending on injected voltages together with bus voltages. The load flow analysis is deemed according to the buses i and j. The reactive power fed by the UPFC controller is expressed as:

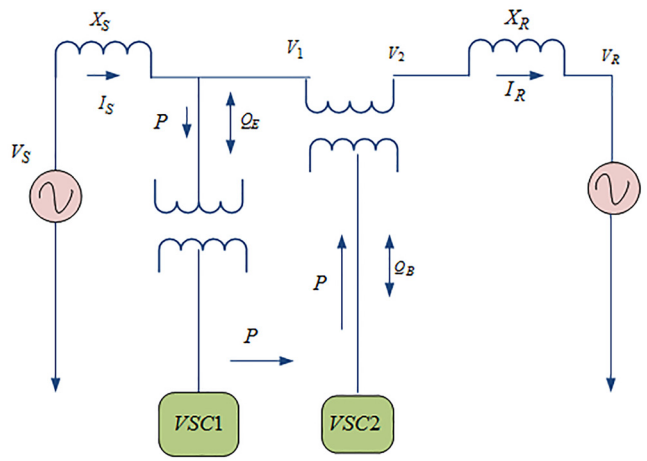

Fig. 3. Block diagram of UPFC controller

$$\frac{dQ_j}{dt} = \frac{dQ_j}{d\delta}\frac{d\delta}{dt} + \frac{dQ_j}{dV_{m2p}}\frac{dV_{m2p}}{dt} \tag{28}$$

From the above equation, it is known that reactive power fed by UPFC is based on V_{m2p} and angle δ and at the point of connection they are proportional to the voltage.

$$\Delta Q_{UPFC} = K_j \Delta\delta(S) + K_k \Delta V(S) \tag{29}$$

4. PROPOSED HYBRID TECHNIQUE

The transient stability of grid connected hybrid system is achieved by the Hybrid DMO-RERNN technique which is the joined execution of DMO and RERNN. Here, the DMO is utilized to find global optimum solution for the proposed system and RERNN is used to predict the fault in the system.

4.1. Dwarf mongoose optimization algorithm (DMO)

DMO is a novel metaheuristic method based on adaptive behavior of dwarf mongoose. The proposed DMO is used to determine global optimum solutions for various optimization issues [40]. The optimization process is obtained by designing three structural transformations, such as alpha group, babysitters, scout group [41].

Step 1: Initialization

The DMO parameters, such as *peep*, mongoose population (n_{pop}), baby sitters (bs) and exchange criteria are initialized.

Step 2: Fitness calculation

The fitness value of the mongoose is calculated by assigning the time counter "s" value and the alpha based value is calculated as:

$$\alpha = \frac{fit_i}{\sum_{i=1}^{n} fit_i} \tag{30}$$

Step 3: Evaluation of sleeping mound

The sleeping mound is calculated in this step which is illustrated as:

$$sm_i = \frac{fit_{i+1} - fit_i}{\max\{|fit_{i+1} - fit_i|\}} \tag{31}$$

Step 4: Average value and movement vector calculation

In this step, the average value of sleeping mound and movement vector is determined using the below equation:

$$\varphi = \frac{\sum_{i=1}^{n} sm_i}{n} \tag{32}$$

$$\overrightarrow{M} = \sum_{i=1}^{n} \frac{Y_i \times sm_i}{Y_i} \tag{33}$$

Step 5: Position update

The baby sitter is exchanged if the fitness function value is lesser than or similar with alpha value. The scout mongoose next best position is updated.

Step 6: Termination

Once the best solution is found out the process will terminate. Table 1 tabulates the pseudo code for DMO algorithm.

4.2. Recalling enhanced recurrent neural network (RERNN)

The structure of RERNN contains Input, State, Hidden, Output, and Delay Layer. Figure 4 depicts RERNN using several inputs and outputs. The steps and structure of RERNN are briefly described as below,

Step 1: Initiation

Initiate EV parameters, as count of nodes, vectors weight, count of hidden nodes and count of iteration.

Step 2: Random generation

After the initiation method, the input vectors are generated randomly. At same time, the input parameter of the EV system, like SOC of battery, engine speed, etc. are created randomly.

Step 3: Check iteration

The iteration of the method is less when compared with maximal repetition then the data process will terminate.

Step 4: Find learning rate by generalized Armijo search

The learning rate is determined according to Armijo search method and the equation is expressed as:

$$e\left(W^K + l_r P^K\right) \le e\left(W^K\right) + \alpha_1 l_r e_W^K \left(P^K\right)^T, \alpha_1 \ge 0 \tag{34}$$

Step 5: Calculate new weight

It is utilized to find out the new weight and it is computed depending on following equation,

$$W^{k+1} = W^k + l_R p^k \tag{35}$$

Table 1. Pseudocode for DMO algorithm

begin
Initiate algorithm:
[peep]
Initiate mongoose populations (search agents): m
Initiate number of babysitters: bs
Set $m = m - bs$
Set exchange parameter L
For *iter=1:max_iter*
Compute mongoose fitness
Set time counter C
Find alpha value
$\alpha = \frac{fit_i}{\sum_{i=1}^{n} fit_i}$
Produce candidate food location
$Y_{i+1} = Y_i + phi * peep$
Evaluate a novel fitness of X_{i+1}
Evaluate sleeping mount with the following eqn
$sm_i = \frac{fit_{i+1} - fit_i}{\max\{fit_{i+1} - fit_i\}}$
Compute the average values of sleeping mound $\varphi = \frac{\sum_{i=1}^{n} sm_i}{n}$
Compute movement vector $\vec{M} = \sum_{i=1}^{n} \frac{Y_i \times sm_i}{Y_i}$
Interchange babysitters if $C \geq L$, *and set*
Initialize bs *position and calculate fitness*
$fit_i \leq \alpha$
Put on the scout mongoose next position

$$X_{i+1} = \begin{cases} Y_i - CF * rand * \left[Y_i - \vec{M} \right] & if\ \varphi_{i+1} > \varphi_i \quad Exploration \\ Y_i + CF * rand * \left[Y_i - \vec{M} \right] & else \quad Exploitation \end{cases}$$

Update best solution
End for
Return *best solution*
End

Step 6: Verify the maximum iteration

It attains the maximal iteration process will stop or the iteration value will maximize and goes with step 6.

Step 7: Calculate direction

The calculation of directional learning method takes place with conjugate gradient descent method.

$$P^k = -F_w^k + \beta P^{k-1} \tag{36}$$

$$\beta = \frac{\alpha F_w^k \left(P^{k-1}\right)^t}{P^{k-1}\left(P^{k-1} - F_W^k\right)}, \alpha \in (0,1) \tag{37}$$

Figure 5 portrays flow chart of RERNN method.

5. RESULT AND DISCUSSION

Here, the transient response of grid connected Wind-Diesel-photovoltaic hybrid system is described. The system is analyzed under two cases: (i) constant irradiation with grid fault and (ii) irradiation variation with grid fault.

Case 1: Constant Irradiation with grid fault

The analysis of distribution generation active power and reactive power is represented in Fig. 6. In Fig. 6 (a), the DGs active power value is 2,500 W and it remains constant with slight variation. Figure 6 (a) displays the reactive power of DGs is 1,400 W and remains constant with slight variation. The analysis of distribution generation current and voltage is shown in Fig. 7. In Fig. 7 (a), the current of DGs during constant irradiation varies from −3 to 3 A. In Fig. 7 (b), the voltage of the DGs during constant irradiation deviates from −500 to 500 A. Figure 8 displays the analysis of distribution generation grid active and reactive power comparison. Under constant irradiation the grid active of the DG is 5 W through the time interval of 0–0.15 time/sec and decrease to 0.3 W and again increases to 3.8 W at 0.15 time/sec. Figure 8 (a) represents the active power value slightly deviate at 0.16 to 0.205 time/sec and remains constant at 4.9 A for the remaining time period. The comparison of grid active power of DMO-RERNN with existing PI, ANN, Fuzzy sliding mode is illustrated in Fig. 8 (b). It is proved that the grid active power of DMO-RERNN is higher than the existing methods.

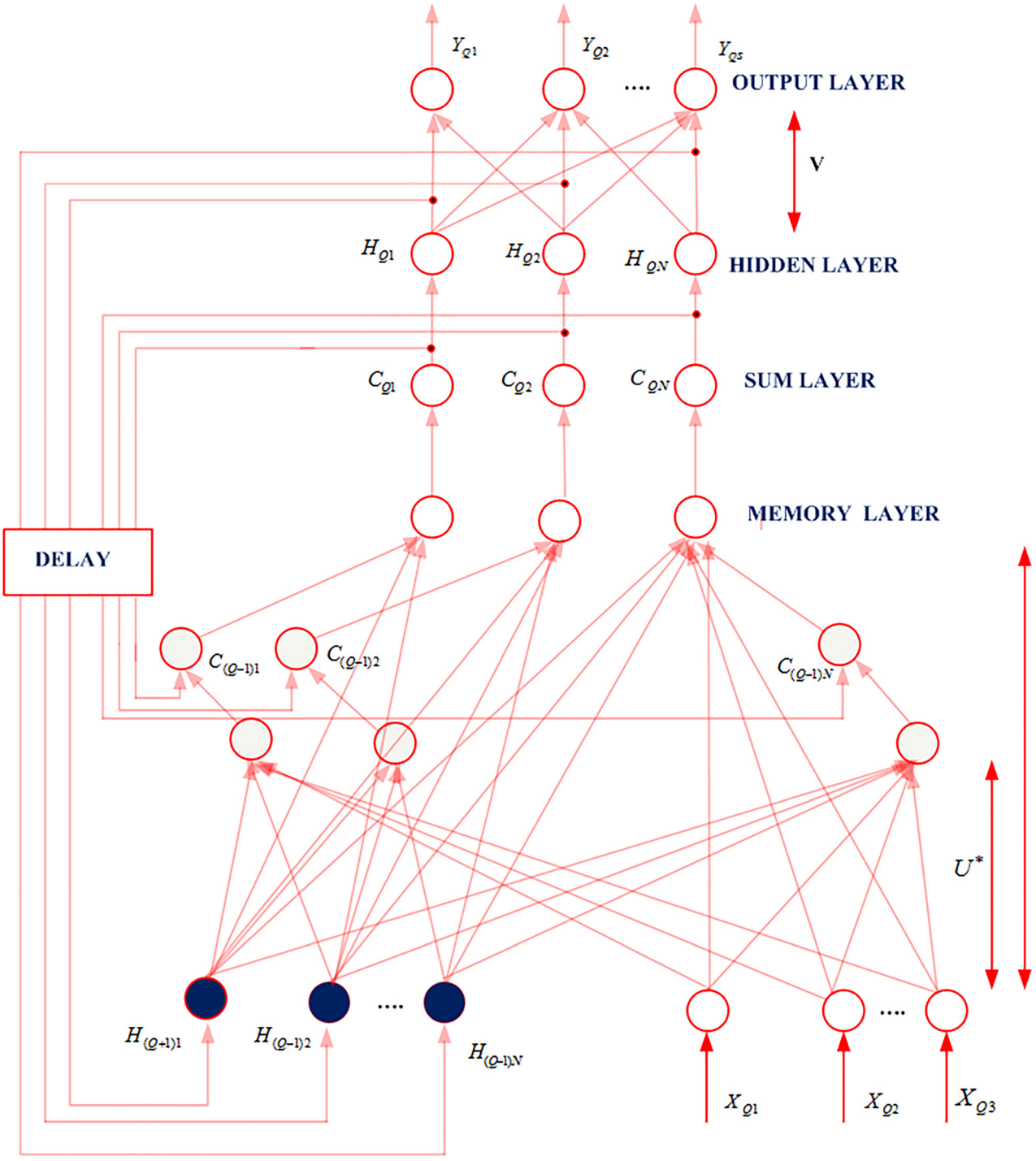

Fig. 4. The RERNN structure with several inputs and outputs

The performance of grid current with voltage is represented in Fig. 9. During constant irradiation the grid current value differs from −1,000 to 1,000 A and there is a deviation present at 0.15 to 0.2 time/sec which is shown in Fig. 9 (a). During constant irradiation the grid voltage varies from −3,000 to 3,000 V and during the time period of 0.15–0.2 time/sec which is displayed in Fig. 9 (b). The PV current and voltage analysis during constant irradiation is represented in Fig. 10. In Fig. 10 (a), the current produced from the PV increases from 0 to 11 A at 0 to 0.02 time/sec leftovers stable for the remaining time period. Figure 10 (b) portrays PV voltage increase 0–5,100 W at 0 to 0.02 time/sec leftovers stable with slight variation for the remaining time period.

The estimation of PV power and comparison of PV power demonstrated in Fig. 11. In Fig. 11 (a), the power value of PV emerges from 0 to 5,500 W at 0 to 0.02 time/sec leftovers

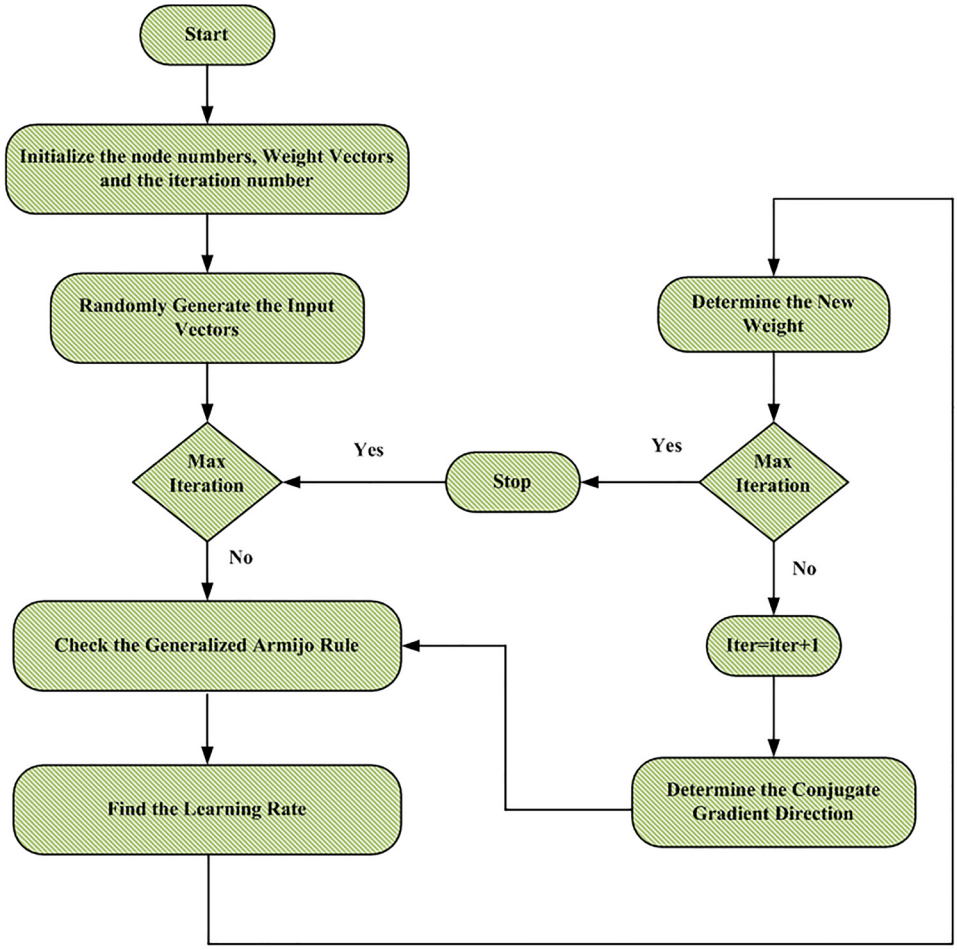

Fig. 5. Flowchart of RERNN

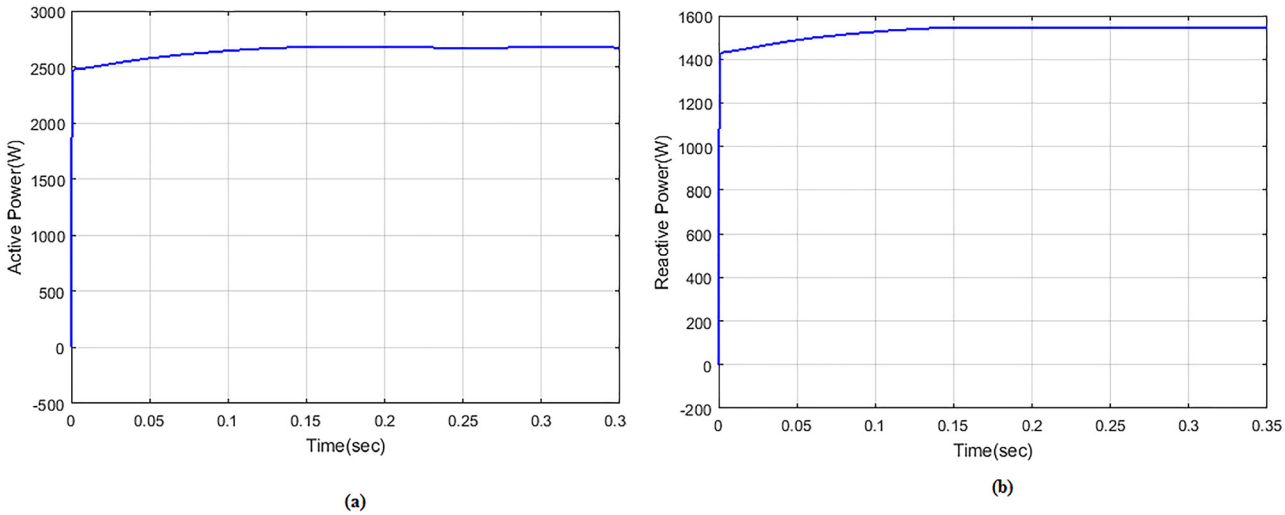

Fig. 6. Analysis of distribution generation (a) active power (b) reactive power

constant for the rest of the time. Figure 11 (b) illustrates that the DMO-RERNN power is superior to existing systems. The analysis of wind current and voltage is depicted in Fig. 12. In Fig. 12 (a), wind current oscillates from −3–3.5 A during the interval of 0–0.02 time/sec. In Fig. 12 (b), the voltage produced from wind oscillates from −450 to 450 at 0 to 0.02

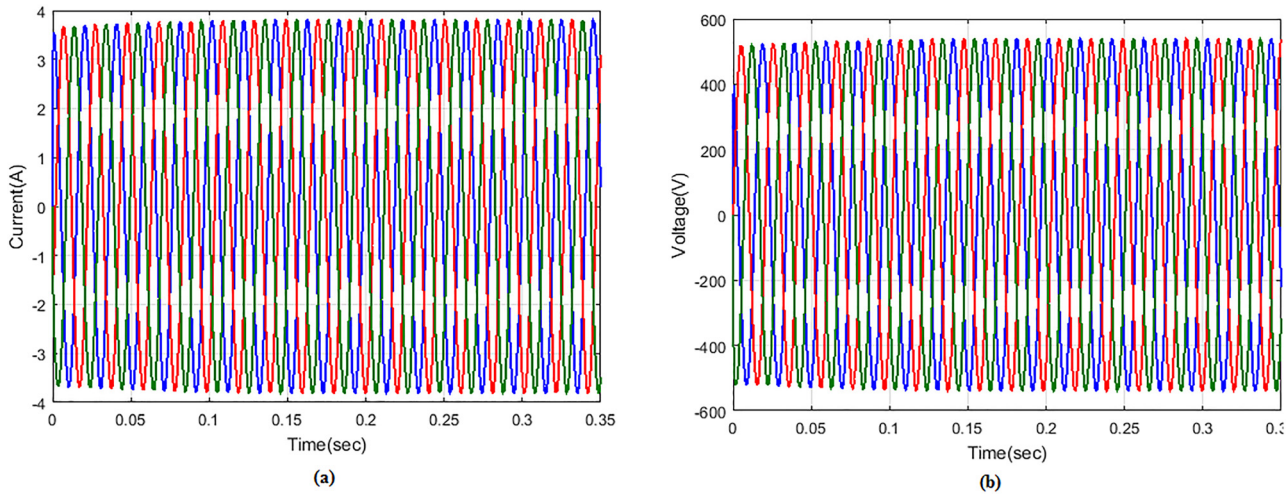

Fig. 7. Estimation of distribution generation (a) current (b) voltage

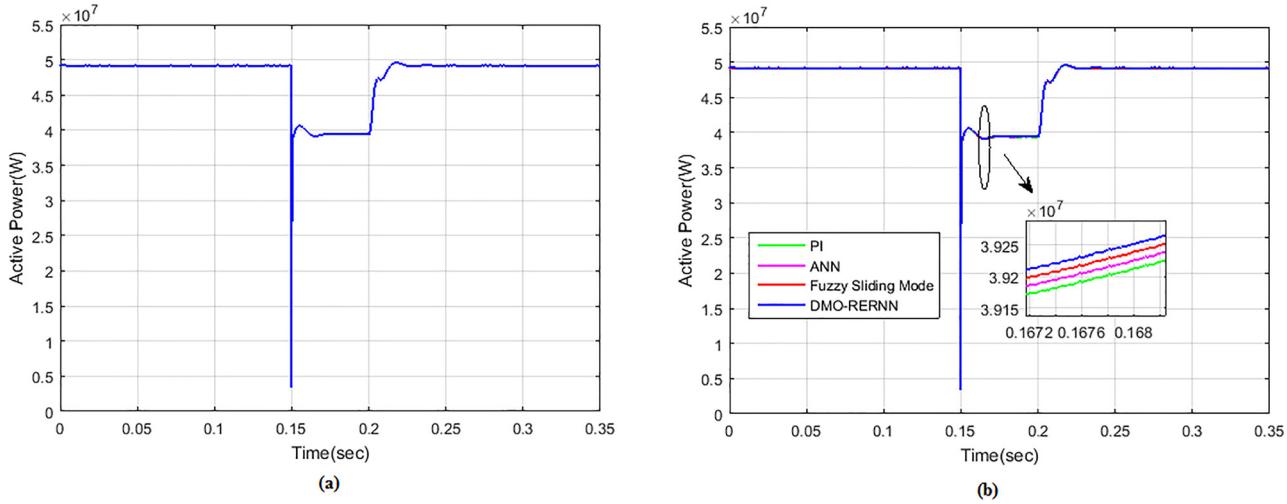

Fig. 8. Estimation of distribution generation (a) grid active power (b) grid active power comparison

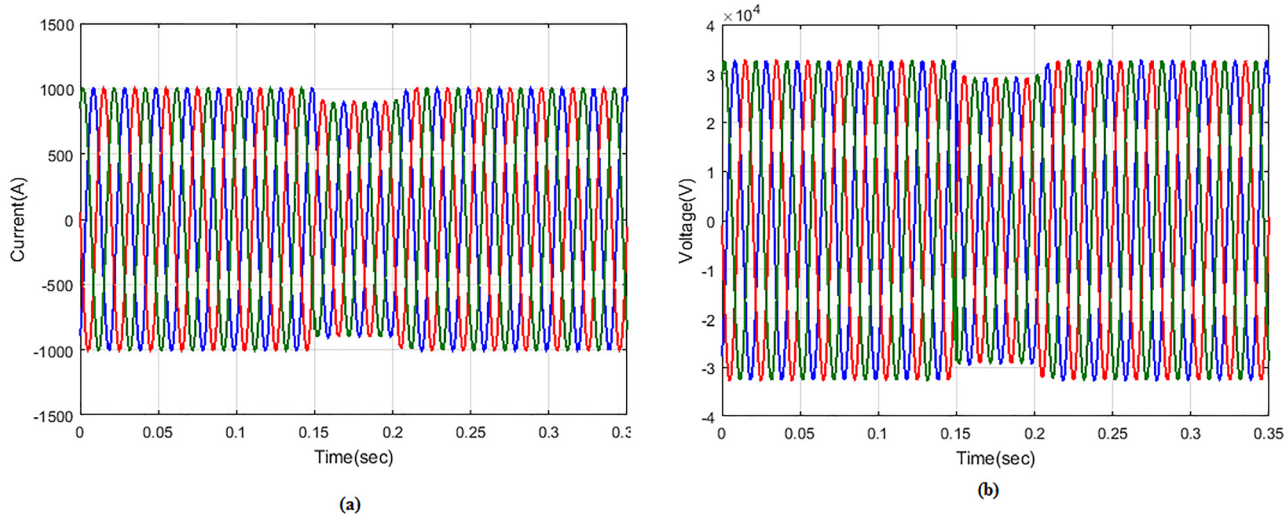

Fig. 9. Estimation of grid (a) current (b) voltage

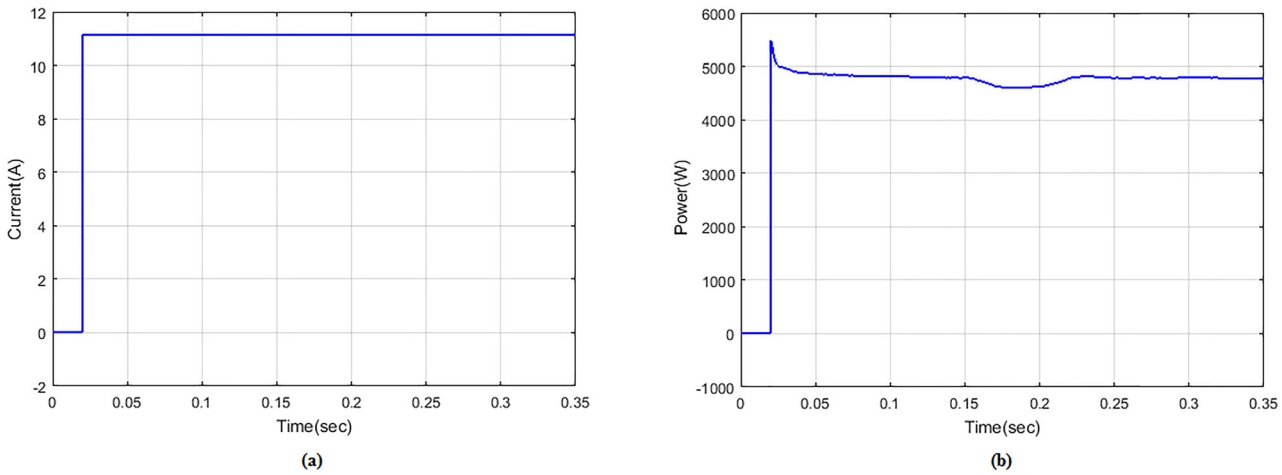

Fig. 10. Analysis of PV (a) current (b) power

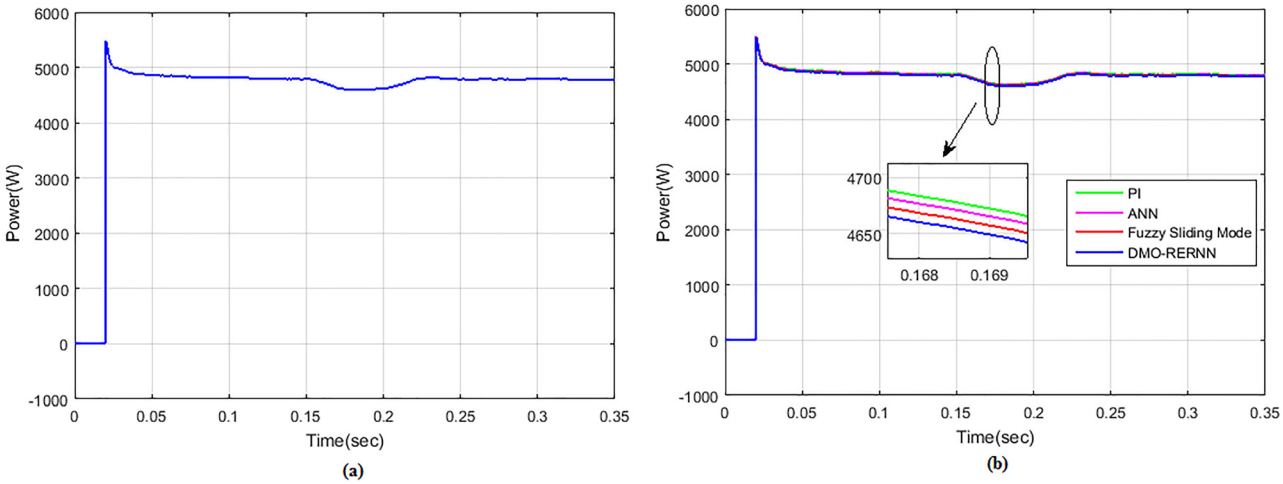

Fig. 11. Analysis of PV (a) Power (b) Power comparison in case 1

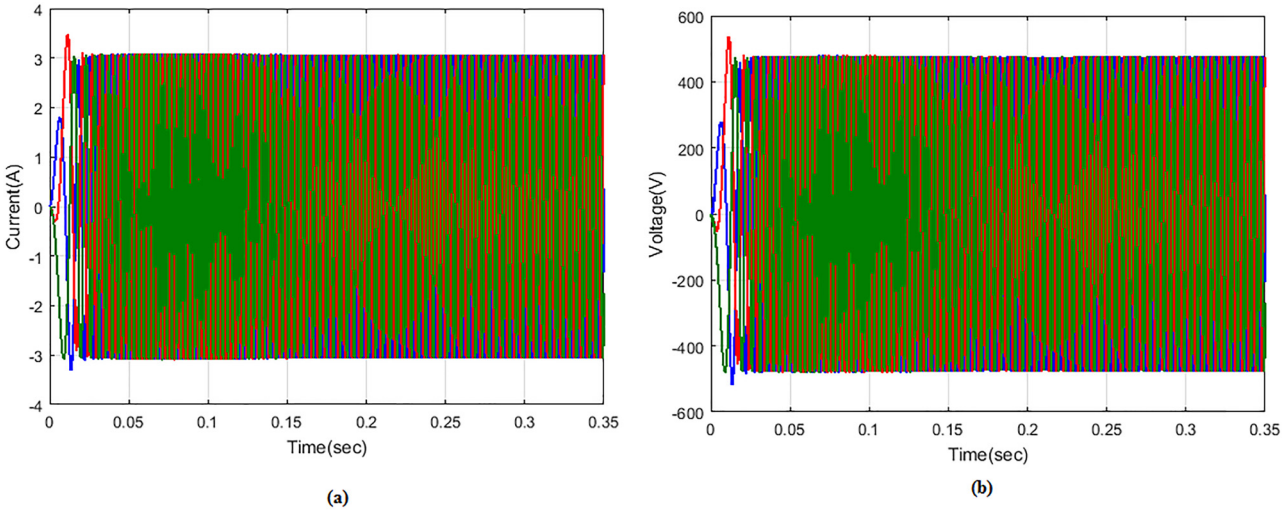

Fig. 12. Estimation of Wind (a) current (b) voltage

time/sec. The analysis of wind active power and the comparison are represented in Fig. 13. In Fig. 13 (a), the wind active power maximizes from 0 to 2,700 W at 0 to 0.02 time/sec. again, it drops to 2,000 W and increases to 2,100 W at 0.02 to 0.03 time/sec and remains constant for the rest of the time. The comparison graph shows that the wind active power of DMO-RERNN is higher than the existing PI, ANN and fuzzy sliding mode represented in Fig. 13 (b).

Case 2: Irradiation variation with grid fault

The analysis of distribution generation active and reactive power during irradiation variation with grid fault is demonstrated in Fig. 14. In Fig. 14 (a), the DGs active power value is 2,500 W and it remains constant with slight variation. In Fig. 14 (b), the reactive power of the DGs is 1,400 W and remains constant with slight variation. The analysis of distribution generation current and voltage during irradiation variation with grid fault is shown in Fig. 15. In Fig. 15 (a), the current of the DGs during irradiation variation varies from −3.5 to 3.5 A. In Fig. 15 (b), the voltage of the DGs during irradiation variation deviates from −500 to 500 A. The analysis of distribution generation grid active power and the comparison of grid active power are shown in Fig. 16. Under irradiation variation condition the grid active power of the DG is 5 W at 0 to 0.15 time/sec and decreases to 3 W. Then it increases to 3.2 W at 0.16 time/sec again it emerges to 4 W and then to 5 W in the time duration of 0.21–0.28 time/sec. For the remaining time period it remains constant which is displayed in Fig. 16 (a). The grid active power of DMO-RERNN with existing PI, ANN, Fuzzy sliding mode is illustrated in Fig. 16 (b). It is proved that the grid active power of DMO-RERNN is higher to existing systems.

The analysis of grid current and voltage represented in Fig. 17. In Fig. 17 (a), during irradiation variation the grid

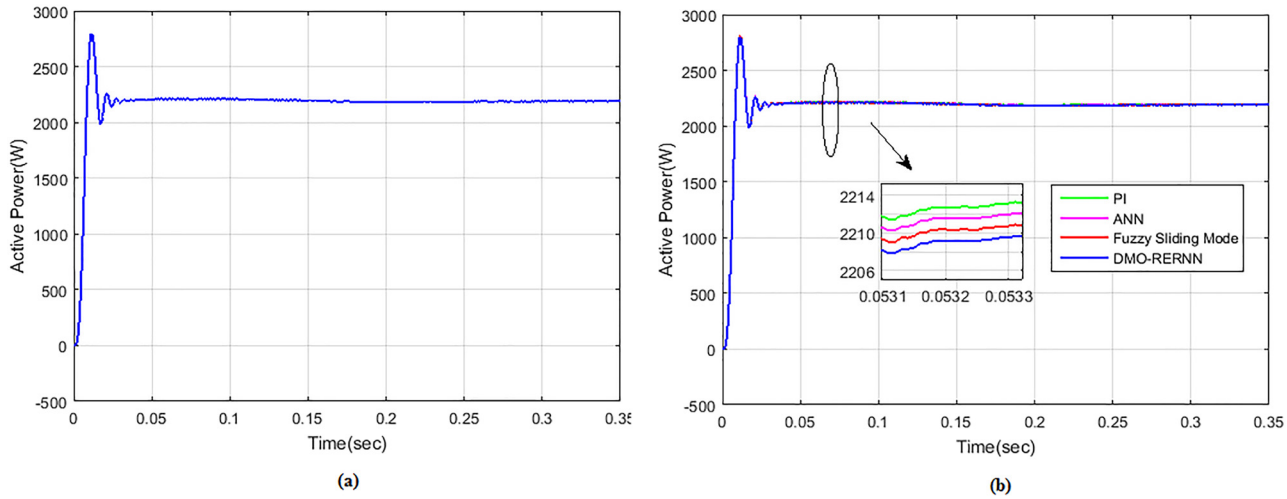

Fig. 13. Estimation of Wind (a) active power (b) active power comparison

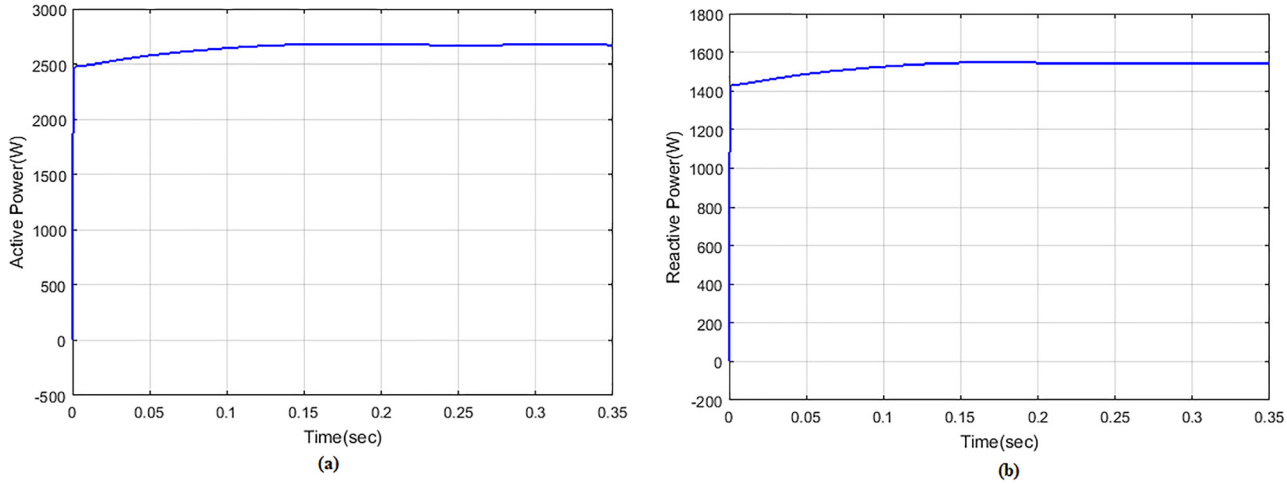

Fig. 14. Analysis of distribution generation (a) active (b) reactive power

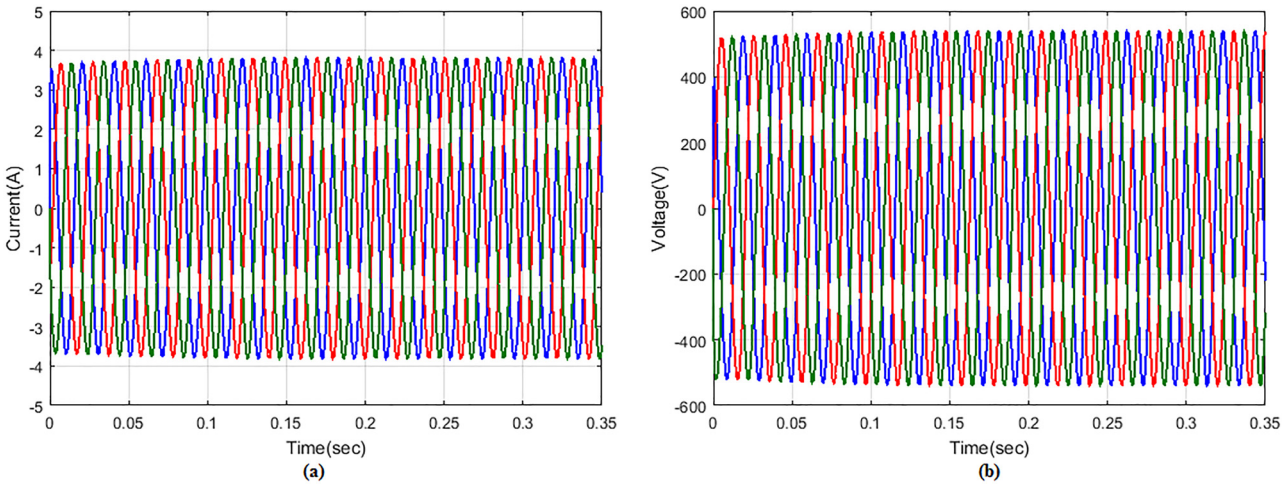

Fig. 15. Analysis of distribution generation (a) current (b) voltage

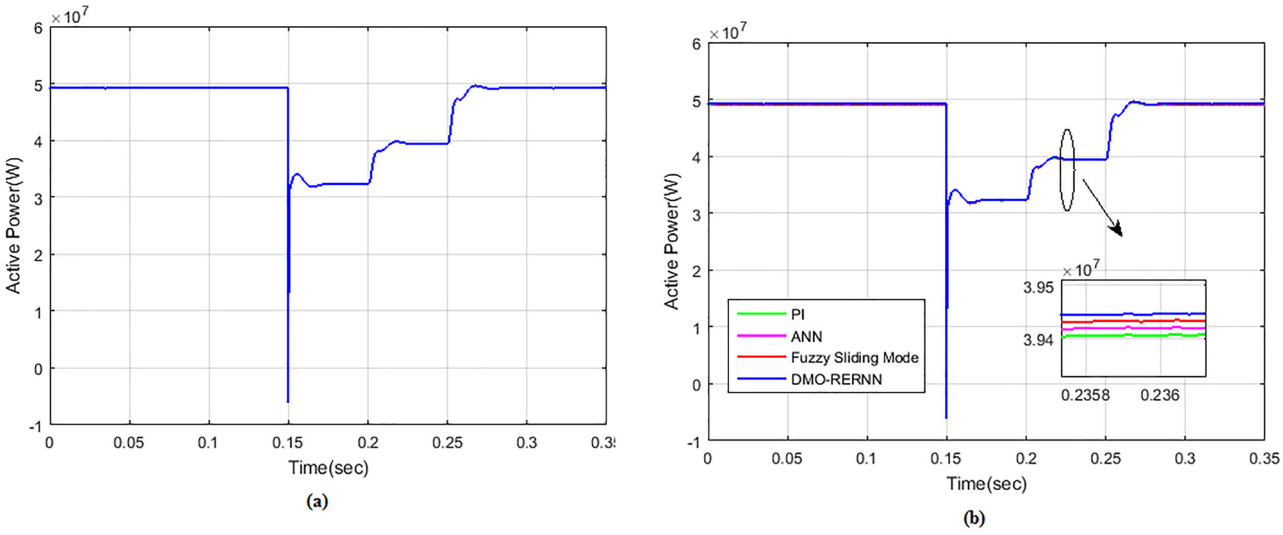

Fig. 16. Analysis of distribution generation (a) grid active power (b) comparison of grid active power

current value differs from −1,000 to 1,000 A and there is a deviation present at 0.15 to 00.25 time/sec. The grid voltage varies from −3,000 to 3,000 V during the time period of 0.15–0.27 time/sec is displayed in Fig. 17 (b). Figure 18 displays the analysis of reactive power, in which the reactive power value is 4 W at 0 to 0.15 time/sec, then there is sudden drop to 0.9 W AT 0.15 time/sec. Again, the reactive power rises to 2.6 A and it gradually rises with the presence of slight oscillation for the remaining time period. The analysis of PV current and voltage during irradiation variation condition is represented in Fig. 19. In Fig. 19 (a), the current produced from PV increases 0–6.4 A at 0 to 0.02 time/sec leftovers stable during 0.02–0.2 time/sec. Again, it rises to 9 A during 0.2–0.21 time/sec leftovers stable at 0.21 to 0.3 time/sec then increases to 11 A leftovers stable. Figure 19 (b) shows PV voltage increase 0–350 W at 0 to 0.02 time/sec and there is an oscillation for the remaining time period. The analysis of PV current and voltage during irradiation variation condition is represented in Fig. 19. In Fig. 19 (a), the current produced from the PV increases from 0 to 6.2 A at 0 to 0.02 time/sec leftovers stable at 0.02 to 0.2 time/sec and it increases gradually during the time duration of 0.2–0.3 time/sec. Figure 19 (b) shows that PV voltage increase from 0 to 350 V at 0 to 0.02 time/sec there is a slight deviation for the remaining time period.

The PV power analysis and comparison of PV power is illustrated in Fig. 20. In Fig. 20 (a), the power value of PV emerges from 0 to 2,300 W during 0–0.02 time/sec leftovers stable during 0.02–0.15 time/sec, then it gradually increases for the rest of the time. Figure 20 (b) illustrates that the DMO-RERNN method power is higher to existing systems like proportionate integral (PI), artificial neural network (ANN) and fuzzy sliding mode.

The analysis of wind active power and the comparison are represented in Fig. 21. In Fig. 21 (a), the wind active power maximizes 0–2,800 W at 0 to 0.02 time/sec, again, it

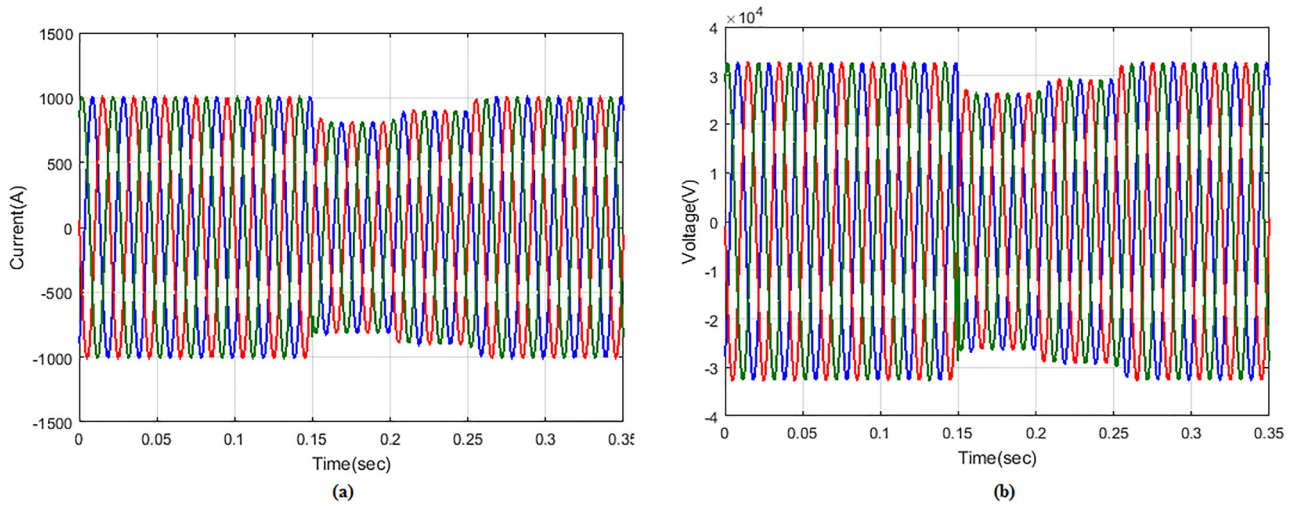

Fig. 17. Analysis of grid (a) current (b) voltage

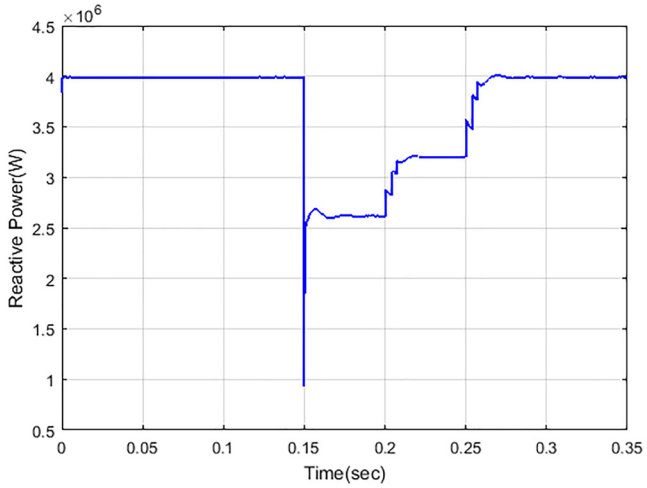

Fig. 18. Estimation of Reactive power

drops to 2,000 W and increases to 2,100 W at 0.02 to 0.03 time/sec and remains constant for the rest of the time. The comparison graph shows that the wind active power of DMO-RERNN is higher than other existing methods, such as PI, ANN and fuzzy sliding mode which represented in Fig. 21 (b). The analysis of wind current and voltage during irradiation variation condition is shown in Fig. 22. In Fig. 21 (a), the wind current oscillates from −3–3.5 A during the interval of 0–0.02 time/sec. In Fig. 21 (b), the wind voltage oscillates from −450 to 450 at 0 to 0.02 time/sec. Efficiency comparison of source power is shown in Table 2. For 100 iterations first order statistic is given in Table 3. Computation time with numerous numbers of trails of proposed and existing systems is shown in Table 4.

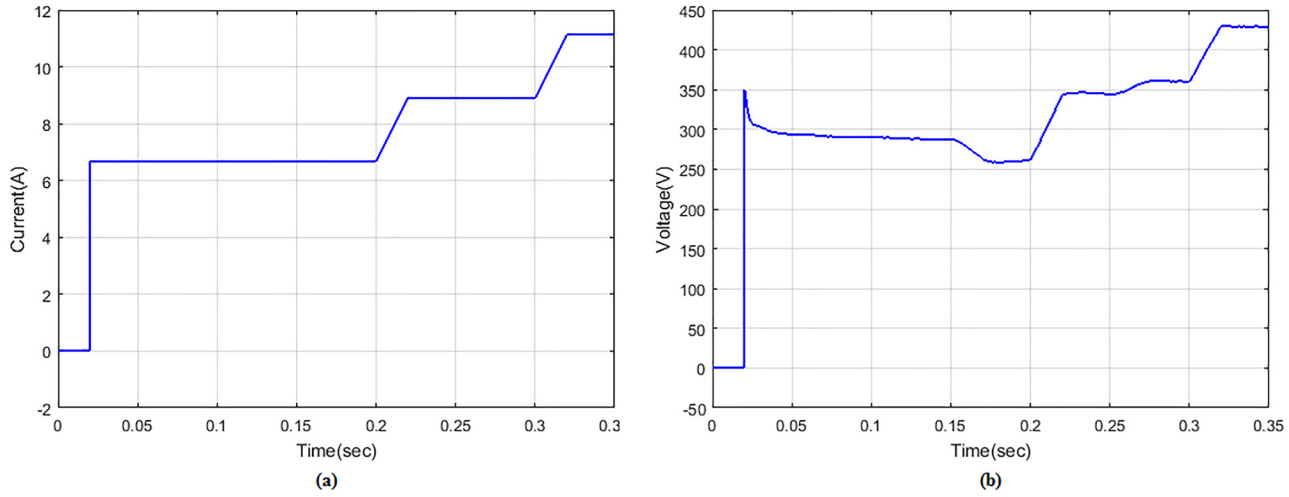

Fig. 19. Analysis of PV (a) current (b) voltage

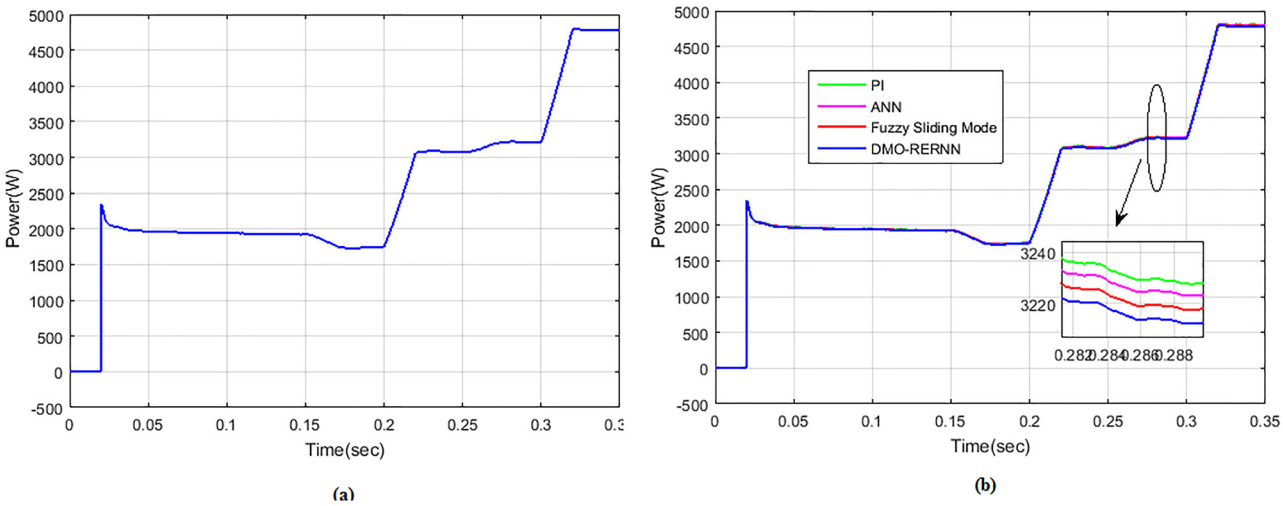

Fig. 20. Analysis of PV (a) Power (b) power comparison in case 2

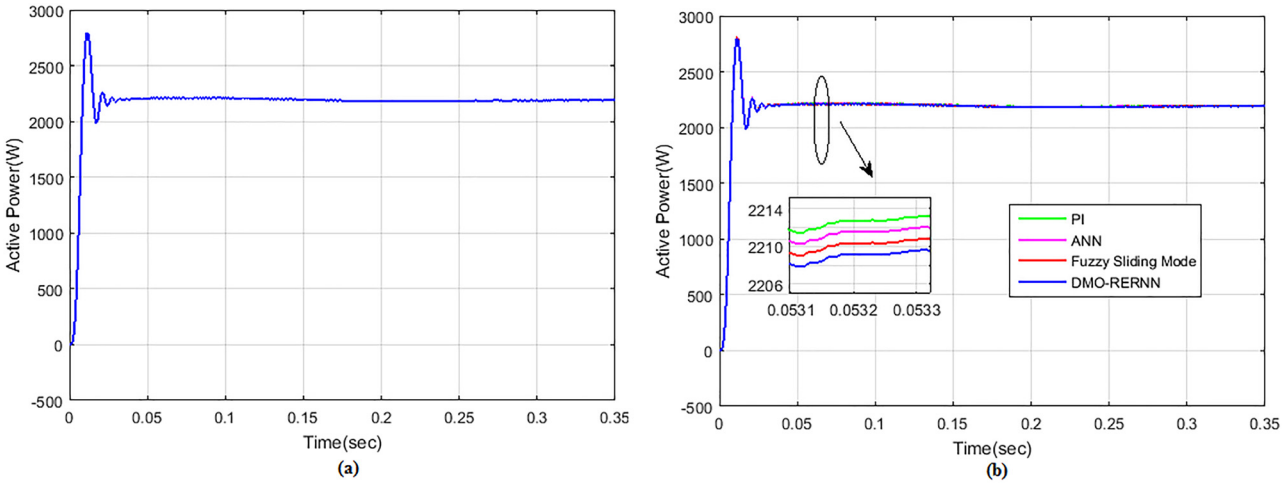

Fig. 21. Analysis of Wind (a) active power (b) active power comparison

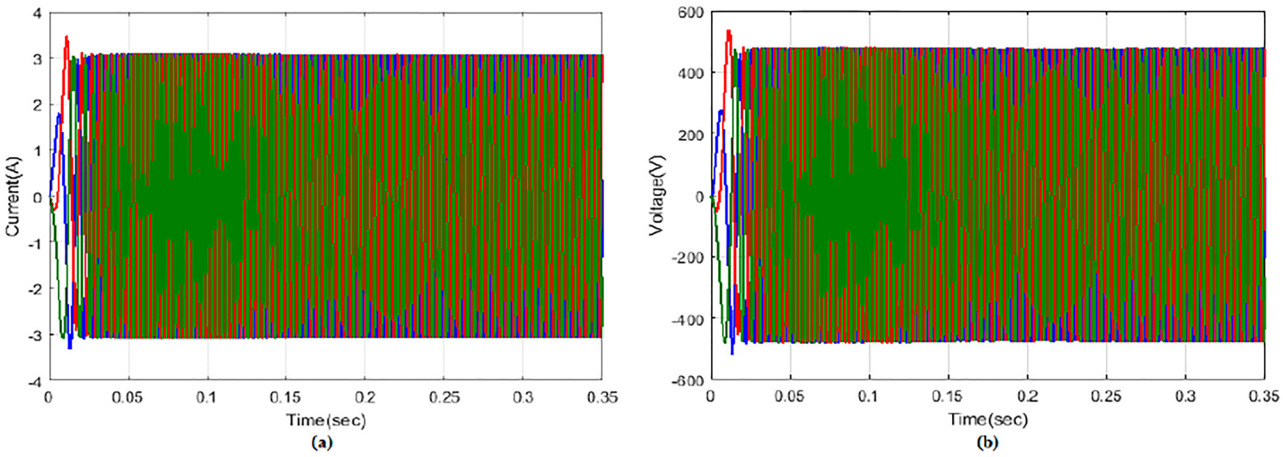

Fig. 22. Analysis of Wind (a) current (b) voltage

Table 2. Efficiency comparison of proposed and existing system

Solution techniques	Efficiency (%)
PI	82.136
ANN	77.26588
Fuzzy Sliding Mode	65.097
Proposed technique	97.99038

Table 3. For 100 iterations first order statistic assessment

Solution	Mean	Median	SD
PI	0.8890	0.8736	0.0061
ANN	0.8514	0.8018	0.0198
Fuzzy Sliding Mode	0.61038	0.5317	0.00543
Proposed system	0.5117	0.4720	0.00417

Table 4. Computation time with several number of trails of proposed and existing systems

Solution techniques	Computation time with several number of trails (sec)				
	100	150	200	250	500
PI	60.0398	70.1257	83.2906	75.9023	75.8707
ANN	57.1107	68.0273	79.0373	69.96800	67.65823
Fuzzy Sliding Mode	48.1740	51.2133	71.0483	60.00126	57.80132
Proposed technique	31.5799	47.0637	65.3690	59.1155	56.0975

6. CONCLUSION

The hybrid system for proper management of reactive power as well as voltage stability enhancement is incorporated with UPFC controller and is simulated through MATLAB platform. The proposed DMO-RERNN based UPFC controller helps to improve the transient stability. The performance of the proposed DMO-RERNN based UPFC controller is analyzed under diverse operating conditions. The simulation outcomes show that transient stability incorporated with proposed DMO-RERNN based UPFC controller provides better result than the conventional ANN, PI and fuzzy-SMC. The system is analyzed under two cases like constant irradiation with grid fault and irradiation variation with grid fault. The system parameters like active and reactive power, DG current and voltage, grid current and voltage, are also analyzed in this proposed work. From this analysis, the proposed work provides the best solution with higher efficiency. Exactly, attention must be paid to transient stability of multi-inverter, multi-machine hybrid systems. The damping effect must no longer be ignored while executing TSA is required. Frequency hopping must also be deemed for determining CCA and CCT. This carries a novel impulse to relay protection design.

Funding Information: This research did not receive any specific grant from funding agencies in the public, commercial, or not-for-profit sectors.

REFERENCES

[1] S. K. Kim, J. H. Jeon, C. H. Cho, E. S. Kim, and J. B. Ahn, "Modeling and simulation of a grid-connected PV generation system for electromagnetic transient analysis," *Solar Energy*, vol. 83, no. 5, pp. 664–78, 2009. https://doi.org/10.1016/j.solener.2008.10.020.

[2] O. C. Onar, M. Uzunoglu, and M. S. Alam, "Modeling, control and simulation of an autonomous wind turbine/photovoltaic/fuel cell/ultra-capacitor hybrid power system," *J. Power Sourc.*, vol. 185, no. 2, pp. 1273–83, 2008. https://doi.org/10.1016/j.jpowsour.2008.08.083.

[3] R. C. Bansal and T. S. Bhatti, "Reactive power control of autonomous wind-diesel hybrid power systems using simulink," *Electric Power Components Syst.*, vol. 35, no. 12, pp. 1345–66, 2007. https://doi.org/10.1080/15325000701426096.

[4] P. Rajesh, F. H. Shajin, B. Rajani, and D. Sharma, "An optimal hybrid control scheme to achieve power quality enhancement in micro grid connected system," *Int. J. Numer. Model. Electron. Networks, Devices Fields*, p. e3019, 2022. https://doi.org/10.1002/jnm.3019.

[5] F. H. Shajin, P. Rajesh, and M. R. Raja, "An efficient VLSI architecture for fast motion estimation exploiting zero motion prejudgment technique and a new quadrant-based search algorithm in HEVC," *Circuits, Systems, Signal Process.*, vol. 41, no. 3, pp. 1751–74, 2022. https://doi.org/10.1007/s00034-021-01850-2.

[6] P. Rajesh, F. H. Shajin, and N. Vijaya Anand, "An efficient estimation model for induction motor using BMO-RBFNN technique," *Process Integration and Optimization for Sustainability*, vol. 5, no. 4, pp. 777–92, 2021. https://doi.org/10.1007/s41660-021-00177-4.

[7] F. H. Shajin, P. Rajesh, and S. Thilaha, "Bald eagle search optimization algorithm for cluster head selection with prolong lifetime in wireless sensor network," *J. Soft Comput. Eng. Appl.*, vol. 1, no. 1, p. 7, 2020.

[8] R. C. Bansal, T. S. Bhatti, and D. P. Kothari, "Automatic reactive power control of isolated wind-diesel hybrid power systems for variable wind speed/slip," *Electric Power Compon. Syst.*, vol. 32, no. 9, pp. 901–12, 2004. https://doi.org/10.1080/15325000490253542.

[9] R. C. Bansal, "Modelling and automatic reactive power control of isolated wind-diesel hybrid power systems using ANN," *Energy Convers. Manage.*, vol. 49, no. 2, pp. 357–64, 2008. https://doi.org/10.1016/j.enconman.2007.06.004.

[10] D. J. Lee and L. Wang, "Small-signal stability analysis of an autonomous hybrid renewable energy power generation/energy storage system Part I: time-domain simulations," *IEEE Trans. Energy Convers.*, vol. 23, no. 1, pp. 311–20, 2008. https://doi.org/10.1109/TEC.2007.914309.

[11] J. K. Kaldellis, D. Zafirakis, and K. Kavadias, "Techno-economic comparison of energy storage systems for island autonomous electrical networks," *Renew. Sustain. Energy Rev.*, vol. 13, no. 2, pp. 378–92, 2009. https://doi.org/10.1016/j.rser.2007.11.002.

[12] S. S. Murthy, O. P. Malik, and A. K. Tandon, "Analysis of self-excited induction generators," *IEE Proc. C Generation, Transm. Distribution*, vol. 129, no. 6, p. 260, 1982. https://doi.org/10.1049/ip-c.1982.0041.

[13] J. J. Shea, "Understanding FACTS-concepts and technology of flexible AC transmission systems [Book Review]," *IEEE Electr. Insul. Mag.*, vol. 18, no. 1, pp. 46–46, 2002. https://doi.org/10.1109/MEI.2002.981326.

[14] M. A. Pai, "Energy function analysis for power system stability," *Electric Mach. Power Syst.*, vol. 18, no. 2, pp. 209–10, 1990.

[15] A. E. Hammad and M. El-Sadek, "Application of a thyristor controlled var compensator for damping subsynchronous oscillations in power systems," *IEEE Trans. Power Apparatus Syst.*, vol. 103, no. 1, pp. 198–212, 1984. https://doi.org/10.1109/TPAS.1984.318608.

[16] P. Rao, M. L. Crow, and Z. Yang, "STATCOM control for power system voltage control applications," *IEEE Trans. Power Deliv.*, vol. 15, no. 4, pp. 1311–7, 2000. https://doi.org/10.1109/61.891520.

[17] Improved STATCOM control to improve transient stability of power of a power system using PSO technique", *J. Xidian Univ.*, vol. 15, no. 3, 2021.

[18] R. Pratheeksha and K. M. Kavitha, "Analysis of STATCOM, SVC and UPFC FACTS devices for transient stability improvement in power system," *Int. J. Sci. Res. (IJSR)*, vol. 5, no. 5, pp. 1207–10, 2015.

[19] T. Tsuda, T. Fukami, Y. Kanamaru, and T. Miyamoto, "Performance analysis of the permanent-magnet induction generator under unbalanced grid voltages," *Electr. Eng. Japan*, vol. 161, no. 4, pp. 60–9, 2007. https://doi.org/10.1002/eej.20585.

[20] K. R. Padiyar and R. K. Varma, "Damping torque analysis of static VAR system controllers," *IEEE Trans. Power Syst.*, vol. 6, no. 2, pp. 458–65, 1991. https://doi.org/10.1109/59.76687.

[21] C. A. Canizares, E. Uzunovic, and J. Reeve, "Transient stability and power flow model of the unified power flow controller for various control strategies," *Int. J. Energy Technol. Pol.*, vol. 4, no. 34, p. 349, 2006. https://doi.org/10.1504/IJETP.2006.009978.

[22] H. Liang, Y. Dong, Y. Huang, C. Zheng, and P. Li, "Modeling of multiple master–slave control under Island microgrid and stability analysis based on control parameter configuration," *Energies*, vol. 11, no. 9, p. 2223, 2018. https://doi.org/10.3390/en11092223.

[23] H. Miura and G. Wu, "Voltage stabilization of distribution system integrated by renewable power generations by cooperated control of STATCOM and interconnecting microgrids," *Int. J. Smart Grid Clean Energy*, vol. 3, no. 1, pp. 96–103, 2014.

[24] C. M. Shareef, R. Thota, N. V. Raja, and T. N. Reddy, "Modelling of wind diesel hybrid system for reverse power management using bess," *Int. J. Eng. Comput. Sci.*, 2016.

[25] B. Wang, B. Fang, Y. Wang, H. Liu, and Y. Liu, "Power system transient stability assessment based on big data and the core vector machine," *IEEE Trans. Smart Grid*, vol. 7, no. 5, pp. 2561–70, 2016. https://doi.org/10.1109/TSG.2016.2549063.

[26] A. M. Kassem and A. Y. Abdelaziz, "Firefly optimization algorithm for the reactive power control of an isolated wind-diesel system," *Electric Power Components Syst.*, vol. 45, no. 13, pp. 1413–25, 2017. https://doi.org/10.1080/15325008.2017.1362071.

[27] A. M. Haruni, A. Gargoom, M. E. Haque, and M. Negnevitsky, "Dynamic operation and control of a hybrid wind-diesel stand-alone power systems" in, 2010 Twenty-Fifth Annual IEEE Applied Power Electronics Conference and Exposition (APEC), 2010. https://doi.org/10.1109/APEC.2010.5433675.

[28] S. Shezan, S. Julai, M. A. Kibria, K. R. Ullah, R. Saidur, W. T. Chong, and R. K. Akikur, "Performance analysis of an off-grid wind-PV (photovoltaic)-diesel-battery hybrid energy system feasible for remote areas," *J. Clean. Prod.*, vol. 125, pp. 121–32, 2016. https://doi.org/10.1016/j.jclepro.2016.03.014.

[29] E. Jamil, S. Hameed, and B. Jamil, "Power quality improvement of distribution system with photovoltaic and permanent magnet synchronous generator based renewable energy farm using static synchronous compensator," *Sustainable Energy Tech. Assessments*, vol. 35, pp. 98–116, 2019. https://doi.org/10.1016/j.seta.2019.06.006.

[30] D. J. Lee and L. Wang, "Small-signal stability analysis of an autonomous hybrid renewable energy power generation/energy storage system Part I: time-domain simulations," *IEEE Trans. Energy Convers.*, vol. 23, no. 1, pp. 311–20, 2008. https://doi.org/10.1109/TEC.2007.914309.

[31] F. Baghdadi, K. Mohammedi, S. Diaf, and O. Behar, "Feasibility study and energy conversion analysis of stand-alone hybrid renewable energy system," *Energy Convers. Manage.*, vol. 105, pp. 471–9, 2015. https://doi.org/10.1016/j.enconman.2015.07.051.

[32] A. Agarala, S. S. Bhat, A. Mitra, D. Zychma, and P. Sowa, "Transient stability analysis of a multi-machine power system integrated with renewables," *Energies*, vol. 15, no. 13, p. 4824, 2022. https://doi.org/10.3390/en15134824.

[33] Z. Tian, Y. Shao, M. Sun, Q. Zhang, P. Ye, and H. Zhang, "Dynamic stability analysis of power grid in high proportion new energy access scenario based on deep learning," *Energy Rep.*, vol. 8, pp. 172–82, 2022. https://doi.org/10.1016/j.egyr.2022.03.055.

[34] D. Rakesh Chandra, S. R. Salkuti, and V. Veeramsetty, "Transient stability enhancement of power system with grid connected DFIG based wind turbine," in *Next Generation Smart Grids: Modeling, Control and Optimization*, Singapore, Springer, 2022, pp. 279–95. https://doi.org/10.1007/978-981-16-7794-6_11.

[35] S. A. Lone and M. D. Mufti, "Modelling and simulation of a stand-alone hybrid power generation system incorporating redox flow battery storage system," *Int. J. Model. Simulation*, vol. 28, no. 3, 2008. https://doi.org/10.1080/02286203.2008.11442486.

[36] K. Sapotra, "Modelling and simulation of grid-connected solar-hydro based hybrid power system," *Int. J. Trend Scientific Res. Develop.*, vol. 2, no. 4, pp. 26–31, 2018.

[37] R. Malvia, "Hybrid power system modelling and simulation," *Int. J. Res. Appl. Sci. Eng. Technol.*, vol. 9, pp. 4242–7, 2021.

[38] H. Hinz, "Analysis of a hybrid system for decentralized power generation," *J. Clean Energy Tech.*, vol. 3, no. 1, pp. 12–7, 2015.

[39] O. A. Rasa, "The dwarf mongoose: a study of behavior and social structure in relation to ecology in a small, social carnivore," *Adv. Study Behav.*, pp. 121–63, 1987.

[40] J. O. Agushaka, A. E. Ezugwu, and L. Abualigah, "Dwarf mongoose optimization algorithm," *Comput. Methods Appl. Mech. Eng.*, vol. 391, 2022, Paper no. 114570. https://doi.org/10.1016/j.cma.2022.114570.

[41] T. Gao, X. Gong, K. Zhang, F. Lin, J. Wang, T. Huang, and J. M. Zurada, "A recalling-enhanced recurrent neural network: conjugate gradient learning algorithm and its convergence analysis," *Inf. Sci.*, vol. 519, pp. 273–88, 2020. https://doi.org/10.1016/j.ins.2020.01.045.